Computer simulations of melts of randomly branching polymers

Angelo Rosa' and Ralf Everaers'

Citation: The Journal of Chemical Physics **145**, 164906 (2016); doi: 10.1063/1.4965827
View online: http://dx.doi.org/10.1063/1.4965827
View Table of Contents: http://aip.scitation.org/toc/jcp/145/16
Published by the American Institute of Physics

Computer simulations of melts of randomly branching polymers

Angelo Rosa[1,a] and Ralf Everaers[2,b]
[1]*SISSA (Scuola Internazionale Superiore di Studi Avanzati), Via Bonomea 265, 34136 Trieste, Italy*
[2]*Univ Lyon, Ens de Lyon, Univ Claude Bernard Lyon 1, CNRS, Laboratoire de Physique and Centre Blaise Pascal, F-69342 Lyon, France*

(Received 12 July 2016; accepted 8 October 2016; published online 27 October 2016)

Randomly branching polymers with *annealed* connectivity are model systems for ring polymers and chromosomes. In this context, the branched structure represents transient folding induced by topological constraints. Here we present computer simulations of melts of annealed randomly branching polymers of $3 \le N \le 1800$ segments in $d = 2$ and $d = 3$ dimensions. In all cases, we perform a detailed analysis of the observed tree connectivities and spatial conformations. Our results are in excellent agreement with an asymptotic scaling of the average tree size of $R \sim N^{1/d}$, suggesting that the trees behave as compact, *territorial* fractals. The observed swelling relative to the size of ideal trees, $R \sim N^{1/4}$, demonstrates that excluded volume interactions are only partially screened in melts of annealed trees. Overall, our results are in good qualitative agreement with the predictions of Flory theory. In particular, we find that the trees swell by the combination of modified branching and path stretching. However, the former effect is subdominant and difficult to detect in $d = 3$ dimensions. *Published by AIP Publishing.* [http://dx.doi.org/10.1063/1.4965827]

I. INTRODUCTION

Randomly branched polymers or trees display surprisingly rich physics. In statistical mechanics, lattice trees are believed to fall into the same universality class as lattice animals[1–3] and their critical exponents are related to those of magnetic systems.[4–7] In polymer chemistry, the deliberate (or accidental[8]) incorporation of monomers with higher functionality into the polymerisation processes modifies materials properties.[9,10] In this context, one has to distinguish the environmental conditions under which chains are studied from those under which they are synthesised and where their connectivity is said to be *quenched*. Here we are interested in randomly branched polymers with *annealed* connectivity, whose structure is meant to represent the transient folding of topologically constrained ring polymers[11–17] (Fig. 1) and chromosomes.[18–21] At the light of the recent results by Lang[22] and Smrek and Grosberg[23] who analysed the threadable fraction of the minimal area encircled by non-concatenated ring polymers in melt, it is a non-trivial and still open question if[24] or to which extent[13,25] this analogy[11] holds also for these systems. However, having shown that it provides at least an excellent approximation,[16] we now proceed to analyse in some detail the statistical properties of melts of annealed trees.

As customary in polymer physics,[9,26–28] we are primarily interested in exponents describing how expectation values for observables scale with the weight, N, of the trees,

$$\langle N_{br}(N)\rangle \sim N^{\epsilon}, \tag{1}$$

$$\langle L(N)\rangle \sim N^{\rho}, \tag{2}$$

$$\langle R_g^2(N)\rangle \sim N^{2\nu}, \tag{3}$$

or the path distance l between tree nodes,

$$\langle R^2(l)\rangle \sim l^{2\nu_{\rm path}}, \tag{4}$$

$$\langle p_c(l)\rangle \sim l^{-\nu_{\rm path}(d+\theta_{\rm path})}. \tag{5}$$

Here, $\langle N_{br}(N)\rangle$ denotes the average branch weight, $\langle L(N)\rangle$ the average contour distance or length of paths on the tree, $\langle R_g^2(N)\rangle$ the mean-square gyration radius of the trees, and $\langle R^2(l)\rangle$ and $\langle p_c(l)\rangle$ the mean-square spatial distance and contact probability of nodes as a function of their contour distance, l. For ideal, non-interacting trees[17,29] $\rho = \epsilon = \nu_{\rm path} = 1/2$, $\nu = 1/4$, and $\theta_{\rm path} = 0$. For interacting systems, the only exactly known exponent is $\nu = 1/2$ for self-avoiding trees in $d = 3$ dimensions.[4] The Flory theory provides a simple and insightful description of a wide range of interacting tree systems,[1,15,30,31] but the results are obtained through uncontrolled approximations and rely on the cancellation of large errors.[26,32] For the present problem, Flory theory predicts that trees in a melt ought to behave as compact fractals with $\langle R_g^2(N)\rangle \sim N^{2/d}$ and that trees should swell by a combination of path swelling and modified branching. As plausible as this prediction might be, it needs to be corroborated by more rigorous approaches.

Here we present the, to our knowledge, first computational study of the properties of melts of annealed trees in $d = 2$ and $d = 3$ dimensions. The article is part of a series,[17,33–35] where we use a combination of computer simulations, Flory theory, and scaling arguments to investigate the connectivity and conformational statistics of randomly branched polymers with excluded volume interactions. We employ the same notation, definitions, and numerical methodologies introduced in our previous work[17] on single self-avoiding trees in good solvent, which we briefly summarise in Sections II and III. Results for trees connectivity and spatial conformations are outlined in

[a]Electronic mail: anrosa@sissa.it
[b]Electronic mail: ralf.everaers@ens-lyon.fr

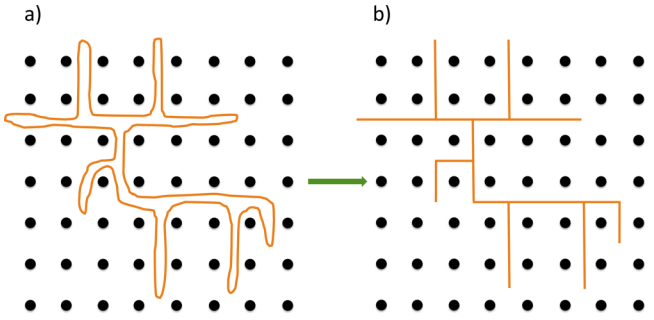

FIG. 1. Behaviour of a two-dimensional ring (orange) in an array of impenetrable fixed obstacles (schematically represented by the black dots). To maximize its conformational entropy, the ring adopts a transiently branched shape (a), which can then be mapped to a lattice tree (b) with *annealed* connectivity. Adapted with permission from Kapnistos *et al.*, Nat. Mater. **7**, 997 (2008). Copyright 2008 Nature Publishing Group.

Sec. IV and discussed in detail in Sec. V. Finally, conclusions are sketched in Sec. VI.

II. MODEL AND BACKGROUND

We are interested in randomly branched polymers with annealed connectivity and repulsive, short-range interactions between monomers. Secs. II A and II B summarize our choices of the employed lattice model, units and notation, and the definition of observables. Sec. II C reviews the predictions of Flory theory for interacting trees. Finally, Secs. II D and II E provide a justification for the model parameters and the sizes of simulated trees by employing the concept of "blob size." All our numerical results are obtained for trees embedded in $d = 2$ and $d = 3$ dimensions, even though many theoretical expressions are conveniently expressed for general d.

A. Model

We study lattice trees on the $2d$- and $3d$-cubic lattice. The functionality of the nodes is restricted to the values $f = 1$ (a leaf or branch tip), $f = 2$ (linear chain section), and $f = 3$ (branch point). Connected nodes occupy adjacent lattice sites. A tree conformation, $\mathcal{T} \equiv (\mathcal{G}, \Gamma)$, can be described by the set of node positions, $\Gamma = \{\vec{r}_1, \ldots, \vec{r}_{N+1}\}$, in the embedding space and a suitable representation of its connectivity graph, $\mathcal{G}$. We employ a data structure in the form of a linked list, which retains for each node, i, its position, $\vec{r}_i$, functionality, f_i, and the indices $\{j_1(i), \ldots, j_{f_i}(i)\}$ of the nodes to which it is connected.

Since our models do not include a bending energy, the lattice constant equals the Kuhn length, l_K, of linear paths across ideal trees. We measure energy in units of k_BT, length in units of the lattice constant or Kuhn length, l_K, and mass in units of the number of Kuhn segments. Similarly, we specify the density by the Kuhn segment number density, ρ_K. We use the letters N and n to denote the mass of a tree or a branch, respectively. With N Kuhn segments connecting the nodes of a tree, there are $N + 1$ nodes in a tree. The symbols L and l are reserved for contour lengths of *linear* paths on the tree, while δL and δl denote contour distances from a fixed point, typically the tree center. Spatial distances are denoted by the letters R and r. Examples are the tree gyration radius, R_g, spatial distances between nodes, $\vec{r}_{ij}$, and the spatial distances, $\vec{\delta r}_i$, of a node from the tree center of mass.

For ideal trees, nodes do not interact and their asymptotic branching probability, λ, is controlled via a chemical potential for branch points,

$$\mathcal{H}_{id}(\mathcal{T}) = \mu_{br} n_3(\mathcal{G}), \tag{6}$$

where $n_3(\mathcal{G})$ is the total number of 3-functional nodes in the tree. All our results are obtained[16] for a value of $\mu_{br} = -2.0\, k_BT$. Interactions between nodes are accounted for via

$$\mathcal{H}_{int}(\mathcal{T}) = v_K \sum_{i \in \, lattice} n_{K,i}^2, \tag{7}$$

where $n_{K,i}$ is the total number of Kuhn segments inside the elementary cell centered at the lattice site i. In all cases we employ the same, large free energy penalty of $v_K = 4\, k_BT$ for overlapping pairs of Kuhn segments, Eq. (7). The pair repulsion is so strong that single trees are effectively self-avoiding, while the local occupancy fluctuations in our melts is $\langle (n_{K,i} - \langle n_{K,i} \rangle)^2 \rangle \approx 0.12 - 0.13$ *for all densities*.

B. Observables

A tree is a branched structure free of loops. Its connectivity can be characterized in a number of ways. Locally, nodes connecting Kuhn segments differ according to their functionality, f, with branch points having functionality $f \equiv 3$ and branch tips $f \equiv 1$. Given n_f the total number of tree nodes with functionality f, they satisfy the relations,

$$n_1 = 2 + n_3, \tag{8}$$

$$n_2 = N - 1 - 2n_3. \tag{9}$$

For our choice of parameters, ideal trees are characterized by an asymptotic branching probability[17]

$$\lambda = \lim_{N \to \infty} \left\langle \frac{n_3(N)}{N} \right\rangle = 0.4. \tag{10}$$

The large scale structure of a tree can be analyzed in terms of the ensemble of sub-trees generated by cutting bonds. Removal of a bond splits a tree of weight N into two trees of weight n and $N - 1 - n$. Defining $N_{br} \equiv \min(n, N - 1 - n)$ as the branch weight, the corresponding ensemble average grows as a characteristic power of the tree weight, $\langle N_{br}(N) \rangle \sim N^{\epsilon}$ (Eq. (1)).

Alternatively, the tree connectivity can be analyzed in terms of (1) the statistics of minimal distances, l_{ij}, of two nodes i, j along linear paths on the tree, and its corresponding ensemble average $\langle L(N) \rangle$, (2) the average distance $\langle \delta L_{\text{center}}(N) \rangle$ of nodes from the central node, and (3) the average length $\langle \delta L_{\text{center}}^{\max}(N) \rangle$ of the longest distance from the central node. For ensemble averages one expects (Eq. (2)) $\langle L(N) \rangle \sim \langle \delta L_{\text{center}} \rangle \sim \langle \delta L_{\text{center}}^{\max}(N) \rangle \sim N^{\rho}$ with[36] $\rho = \epsilon$. Similarly, we characterize the statistics of branches by measuring the average branch weight, $\langle N_{br}(\delta l_{\text{root}}^{\max}) \rangle$, as a function of the *longest* contour distance of nodes from the branch root, $\delta l_{\text{root}}^{\max}(N_{br})$. Finally, we consider the average

weight of the "core" of tree, $\langle N_{center}(\delta l_{\rm center})\rangle$, made of segments whose distance from the central node does not exceed $\delta l_{\rm center}$.

The overall spatial extension of the tree is best described through the mean-square gyration radius $\langle R_g^2\rangle$ which is the average square distance of a node from the tree center of mass. Asymptotically, it is expected to scale as $\langle R_g^2\rangle \sim N^{2\nu}$ (Eq. (3)).

The spatial conformations of linear paths of length l on trees of total mass N can be characterized using standard observables for linear polymers, as follows: (1) the mean-square end-to-end distance $\langle R^2(l,N)\rangle$; (2) for a given contact distance r_c, the corresponding end-to-end closure probability $\langle p_c(l,N)\rangle$. They are expected to scale, respectively, as (Eqs. (4) and (5)) $\langle R^2(l)\rangle \sim l^{2\nu_{\rm path}}$ and $\langle p_c(l)\rangle \sim l^{-\nu_{\rm path}(d+\theta_{\rm path})}$ and to be asymptotically independent of tree weight. By construction,[17] $\nu = \nu_{\rm path}\,\rho$.

C. Flory theory

Flory theories[37] are formulated as a balance of an entropic elastic term and an interaction energy,

$$\mathcal{F} = \mathcal{F}_{el} + \mathcal{F}_{inter}. \tag{11}$$

The central element of the Flory theory of interacting trees is the elastic free energy of ideal annealed trees,[31,38]

$$\frac{\mathcal{F}_{el}}{k_BT} \sim \frac{R^2}{l_K L} + \frac{L^2}{N\,l_K^2}. \tag{12}$$

Ensembles of quenched trees are characterised by fixed values of $L \sim l_K N^{\rho}$ and the Flory energy needs to be minimized over R. Linear chains represent a special case, where $L = l_K N$. In annealed trees, interactions can modify the branching statistics as well as the spatial conformations. With larger contour distances leading to larger spatial distances between repelling monomers, the Flory energy needs to be simultaneously minimized over both variables, R and L. Optimising L for a *given* size, $R \sim N^{\nu}$, yields

$$\rho = \frac{1+2\nu}{3} \tag{13}$$

and

$$\nu_{\rm path} = \frac{3\nu}{1+2\nu}. \tag{14}$$

Thus independently of the physical origin of the effect, swollen trees with $\nu > \nu^{\rm ideal} \equiv 1/4$ are predicted to display both modified connectivities with $\rho > \rho^{\rm ideal} \equiv 1/2$ and path swelling with $\nu_{\rm path} > \nu_{\rm path}^{\rm ideal} \equiv 1/2$.

In melts, volume interactions are screened[1,15] and dominated by high-order collisions of dense systems. Inspecting all terms of order p in a (standard) virial-type expansion of the interaction energy term in Eq. (11),[30]

$$\mathcal{F}_{inter}(N,R) \sim \left(\frac{N}{R^d}\right)^{p-1}, \tag{15}$$

shows that interactions are estimated to be irrelevant, if $\nu d > 1$. Even without swelling, this is the case in $d > 4$ dimensions, where $\nu^{\rm ideal} d = d/4 > 1$ suggests ideal tree behavior. In $d \le 4$ dimensions, for $1/4 < \nu \le 1/d$ the series is dominated by the $p \to \infty$ limit. Minimising the sum of Eqs. (12) and (15) in this limit with respect to L and R yields

$$\nu = \frac{1}{d}, \tag{16}$$

$$\nu_{\rm path} = \frac{3}{d+2}, \tag{17}$$

$$\rho = \frac{d+2}{3d}. \tag{18}$$

Eq. (16)–(18) predict that in the melt state annealed trees are compact fractals. Interestingly, $\nu_{\rm path}$ has the same value as the critical exponent ν for linear self-avoiding walks, suggesting a deeper analogy between the two problems.[15]

D. Blob size

Assuming that entropic effects are too small to induce density inhomogeneities, we can estimate the asymptotic behaviour from the assumption[13] that the asymptotic segment self-density at the tree center of mass converges to the melt segment density ρ_K. More precisely,[16] $\phi \equiv \left(\rho_{tree}\sqrt{(2\pi)^d \det(S)}\right)^{-1} \sim N/R^d/\rho_K \to 1$, where S is the gyration or shape tensor, $S_{\alpha\beta} = \frac{1}{N+1}\sum_{i=1}^{N+1}(\vec{r}_{i\alpha} - \vec{r}_{CM,\alpha})(\vec{r}_{i\beta} - \vec{r}_{CM,\beta})$, and $\vec{r}_{CM}$ is the spatial position of the tree centre of mass. Neglecting asphericity,

$$\langle R_g^2(N)\rangle_{melt} \to \frac{d}{2\pi}\left(\frac{N}{\rho_K}\right)^{2/d}, \tag{19}$$

while our simulation results (Fig. 9(b)) suggest in $d = 3$ with $\langle R_g^2(N)\rangle_{melt} \to 0.59\left(\frac{N}{\rho_K}\right)^{2/3} > \frac{3}{2\pi}\left(\frac{N}{\rho_K}\right)^{2/3} \approx 0.48\left(\frac{N}{\rho}\right)^{2/3}$ a slightly larger value. By using the latter quantity, the blob size,[39]

$$g \approx 0.18\left(\rho_K l_K^3\right)^4/\lambda^3 \tag{20}$$

where we expect the crossover from the ideal to the asymptotic regime to occur is implicitly defined via $\langle R^2(g)\rangle_{ideal} = \langle R^2(g)\rangle_{melt}$ where[29,30] $\langle R^2(g)\rangle_{ideal} = \frac{1}{4}\sqrt{\frac{\pi}{\lambda}} l_K^2 g^{1/2}$. Corresponding arguments in $d = 2$ dimensions yield $\langle R_g^2(N)\rangle_{melt} \to 0.37\frac{N}{\rho_K} > \frac{1}{\pi}\frac{N}{\rho_K} \approx 0.32\frac{N}{\rho_K}$ with a blob size

$$g \approx 1.43\left(\rho_K l_K^2\right)^2/\lambda. \tag{21}$$

E. Choice of simulated tree sizes and segment densities

We have chosen to work with segment densities of $\rho_K l_K^d = 2$, where $g = 14$ in $d = 2$ and $g = 45$ in $d = 3$. With tree sizes up to $N_{max} = 900 \gg g$, we expect to have data sufficiently close to the asymptotic regime for a reliable estimation of the various exponents.

In addition, we have reanalyzed conformations from our original simulation of tree melts in $d = 3$ dimensions.[16] At the time, we used a segment density of $\rho_K l_K^3 = 5$ suggested by the mapping to the corresponding ring polymer problem.

In this case, the estimated blob size of $g = 1758$ equals the size, $N_{max} = 1800$, of the largest trees we were able to simulate, preventing the estimation of asymptotic exponents.

III. METHODS

To simulate melts of annealed lattice trees we have used a variant of the "amoeba" Monte Carlo algorithm by Seitz and Klein[2] (Sec. III A). The quantitative analysis of tree connectivities, tree spatial conformations, and the estimation of critical exponents defined in Eqs. (1)-(4) has been carried out by applying the "burning algorithm"[40,41] (Sec. III B) and ordinary fitting procedures (Sec. III C). Tabulated values and other details on the derivation of critical exponents for single-tree statistics are also reported in the supplementary material.

A. Monte Carlo simulations of annealed tree melts

Amoeba trial moves simultaneously modify the tree connectivity, $\mathcal{G}$, and the tree conformation, Γ. They are constructed by randomly cutting a leaf (or node with functionality $f = 1$) from the tree and placing it on a randomly chosen site adjacent to a randomly chosen node with functionality $f < 3$, to which the leave is then connected. Trial moves, $\mathcal{T}_i \to \mathcal{T}_f$, are accepted with probability,

$$\mathrm{acc}_{i\to f} = \min\left\{1, \frac{n_1(i)}{n_1(f)} e^{-\beta\left(\mathcal{H}(\mathcal{T}_f)-\mathcal{H}(\mathcal{T}_i)\right)}\right\}, \qquad (22)$$

where $n_1(i/f)$ is the total number of 1-functional nodes in the initial/final state and $\mathcal{H}(\mathcal{T}) = \mathcal{H}_{id}(\mathcal{T}) + \mathcal{H}_{int}(\mathcal{T})$, Eqs. (6) and (7). It should be noted that our version of the amoeba algorithm is slightly modified with respect to the original one of Ref. 2 as we impose[16] node functionalities $f \le 3$. Similar algorithms displacing entire branches are more efficient for single trees,[36] but are likely to encounter difficulties when generalized to the dense systems we are mostly interested in. In contrast, the small non-local mass transport of the amoeba algorithm is not obstructed by the volume interactions, since it falls into the range of the natural occupancy fluctuations in our tree melts.

Our simulations start from linearly connected random walks as initial states. The total computational effort for equilibrating the systems as a function of the corresponding systems sizes is summarised in Table SI. As illustrated by Fig. 2, the tree gyration radii equilibrate over a time

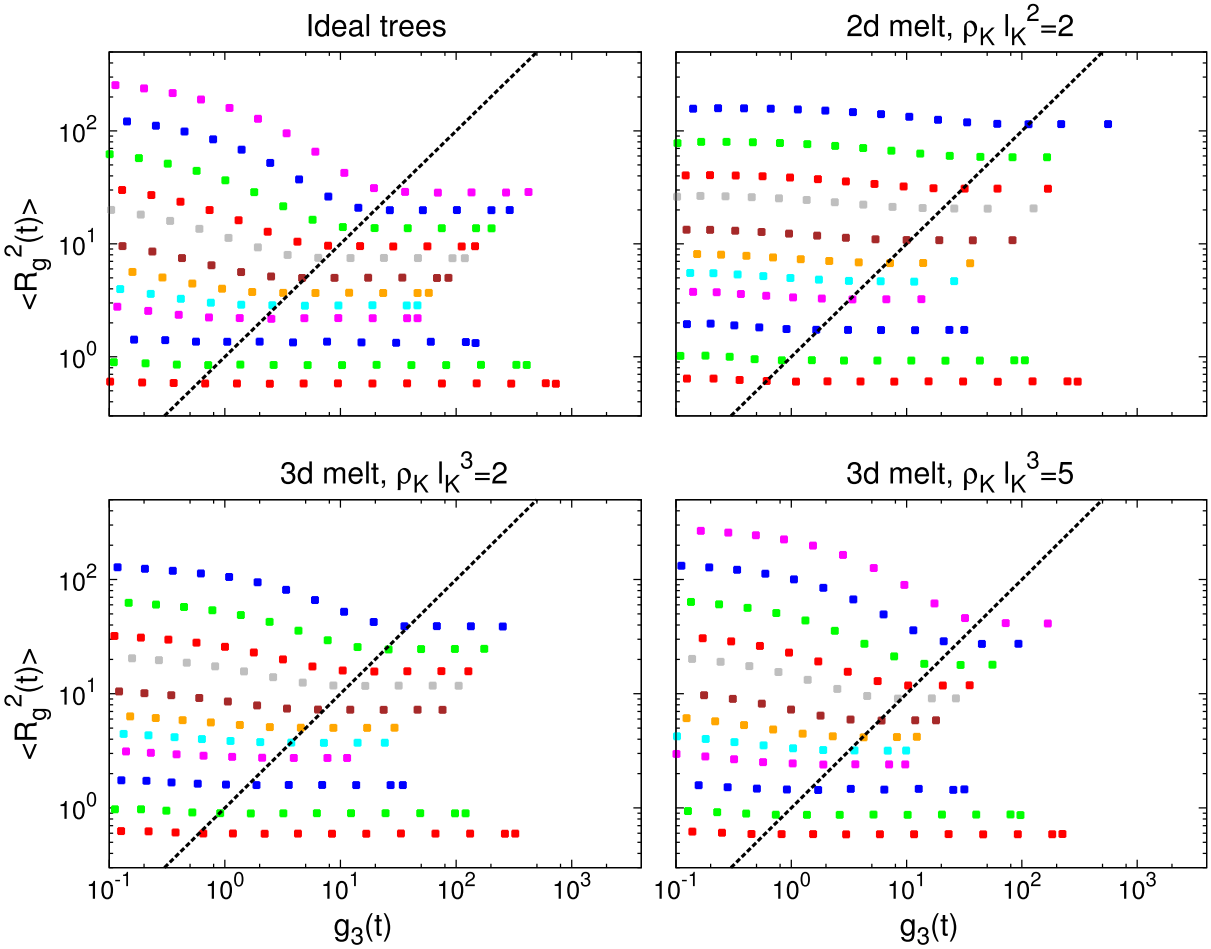

FIG. 2. Parametric plots of the MC-time (t) evolution of the ensemble-average square gyration radius, $\langle R_g^2(t)\rangle$, *vs.* the mean-square displacement of the tree center of mass, $g_3(t)$. Non-equilibrated (respectively, equilibrated) values of the plots correspond to regions above (respectively, below) the black solid line $y = x$. Different colors correspond to different tree masses ranging from (bottom symbols) $N = 3$ to (top symbols) $N = 900$ (melts for $\rho_K l_K^3 = 2$) and $N = 1800$ (ideal trees and melts for $\rho_K l_K^3 = 5$). Top left panel is as in Ref. 17, and reproduced with permission from A. Rosa and R. Everaers, J. Phys. A: Math. Theor. **49**, 345001 (2016). Copyright 2016 IOP Publishing Ltd.

scale during which the tree centers of mass diffuse over the corresponding distance. Quite curiously, the performance of the "amoeba" algorithm as a function of the Monte Carlo time steps is non-monotonic in the system density ρ_K, see Fig. S1. In fact, while $3d$ self-avoiding trees ($\rho_K l_K^3 \to 0$, studied in our previous work[17]) and $3d$ melts for $\rho_K l_K^3 = 5$ take roughly the same time to reach equilibrium, $2d$ and $3d$ tree melts at density $\rho_K l_K^d = 2$ require simulations which are ≈10 times longer. In particular, this is the reason why we have only been able to reach tree weights up to $N_{\max} = 900$ compared to $N_{\max} = 1800$ in Ref. 16. At the moment we have no explanation accounting for this, apparently counterintuitive, behavior.

B. Analysis of tree connectivity

As in our previous work,[17] we have analysed tree connectivities using a variant of the "burning" algorithm for percolation clusters.[40,41] The algorithm is very simple, and consists of two parts. In the initial inward (or burning) pass branch tips are iteratively "burned" until the tree center is reached. In the subsequent outward pass one advances from the center towards the periphery. The inward pass provides information about the mass and shape of branches. The outward pass allows to reconstruct the distance of nodes from the tree center. By employing a data structure in the form of a linked list, which retains for each node, i, its position, $\vec{r}_i$, functionality, f_i, and the indices $\{j_1(i), \ldots, j_{f_i}(i)\}$ of the nodes to which it is connected, each step of the burning algorithm consists in removing from the list all sites with functionality =1 (tips) and updating the functionalities and the indices of the remaining nodes accordingly. The algorithm stops when only one node remains in the list. In order to find the minimal path length l between any pair of tree nodes i and j, we have modified the algorithm by requiring that sites i and j are not removed from the list. Accordingly, the algorithm stops when nodes i and j are the only tips left of the "burned" tree. By using the remaining linked list it is then trivial to find the corresponding path length l.

C. Extracting exponents from data for finite-size trees

In order to get reliable estimates of critical exponents "$\rho, \epsilon, \nu_{\text{path}}, \nu$" in the large-$N$ limit and of the corresponding errors, we stay close to the procedure developed by Janse van Rensburg and Madras[36] and employed in our previous work,[17] and combine the results obtained from fitting the N-dependent data to two functional forms. For the specific example of the exponent ν, they are given by the following expressions:

1. a simple power-law behavior with 2 (a, ν) fit parameters,

$$\log\langle R_g^2(N)\rangle = a + 2\nu \log N, \tag{23}$$

and

2. a power-law behavior with a correction-to-scaling term ($\sim N^{-\Delta_0}$) with 4 (a, b, Δ, ν) fit parameters,

$$\log\langle R_g^2(N)\rangle = a + bN^{-\Delta_0} + 2\nu \log N - b(\Delta - \Delta_0)N^{-\Delta_0} \log N. \tag{24}$$

Here, we have carried out a one-dimensional search for the value of Δ_0 for which the fit yields a vanishing $N^{-\Delta_0} \log N$ term.

For the other exponents, we have employed analogous expressions. Eq. (23) has been used on data with $N \geq 230$ and $N \geq 450$ for $\rho_K l_K^d = 2$ ($d = 2, 3$) and $\rho_K l_K^3 = 5$, respectively. Eq. (24) has been employed on the whole range with $N \geq 10$. Best fits are obtained by minimizing[42] $\chi^2 = \sum_{i=1}^{D} \left[\frac{\log\langle R_g^2(N_i)\rangle_{observed} - \log\langle R_g^2(N_i)\rangle_{model}}{\delta \log\langle R_g^2(N_i)\rangle}\right]^2$, where D is the number of data points used in the fit procedure. Quality of the fit is estimated by the normalized $\tilde{\chi}^2 \equiv \frac{\chi^2}{D-f}$, where f is the number of fit parameters. When $\tilde{\chi}^2 \approx 1$ the fit is deemed to be reliable.[42] The corresponding $Q(D-f, \chi^2)$-values provide a quantitative indicator for the likelihood that χ^2 should exceed the observed value, if the model were correct.[42] All fit results are reported together with the corresponding errors, $\tilde{\chi}^2$ and Q values. Final estimates of critical exponents are calculated as

TABLE I. *Asymptotic* (left) and *crossover* (right) critical exponents for $2d$ and $3d$ lattice trees. (a) ρ, ϵ, ν_{path} and ν: Comparison between predictions of Flory theory and numerical results. As explained in Sec. III C, numerical results for ρ, ϵ, and ν (for this last exponent, with the only exception of $2d$ melts) were derived by combining values and statistical errors of the parameters obtained from best fits (Tables SIV and SVII) of Eqs. (23) and (24) to corresponding observables. For ν_{path} and ν in $2d$ melts, Eq. (24) fails (Table SVII) and only Eq. (23) was employed. (b) θ_{path}: Numerical results are obtained by combining the estimated values of ν_{path} with the values of "$\nu_{\text{path}}\theta_{\text{path}}$" averaged over the ranges of l's where this quantity shows a quasi-plateau for $N = 900$ or $N = 1800$ (see grey and black lines in the insets of the r.h.s panels of Fig. 8): $\nu_{\text{path}}\theta_{\text{path}} = -0.02 \pm 0.02$ (ideal trees); $\nu_{\text{path}}\theta_{\text{path}} = 0.51 \pm 0.05$ ($2d$ melt of trees, $\rho_K l_K^2 = 2$); $\nu_{\text{path}}\theta_{\text{path}} = 0.07 \pm 0.03$ ($3d$ melt of trees, $\rho_K l_K^3 = 2$); $\nu_{\text{path}}\theta_{\text{path}} = 0.08 \pm 0.01$ ($3d$ melt of trees, $\rho_K l_K^3 = 5$). Average values and corresponding error bars have been rounded to the first significant decimal digit.

	Relation to other exponents	Ideal trees with annealed connectivity		$2d$ melt of trees with annealed connectivity		$3d$ melt of trees with annealed connectivity		$3d$ melt of trees with annealed connectivity
		Theory	Simul.	Theory	Simul., $\rho_K l_K^2 = 2$	Theory	Simul., $\rho_K l_K^3 = 2$	Simul., $\rho_K l_K^3 = 5$
ρ	…	$\frac{1}{2} = 0.5$	0.49 ± 0.04	$\frac{2}{3} \approx 0.667$	0.613 ± 0.007	$\frac{5}{9} \approx 0.556$	0.52 ± 0.05	0.53 ± 0.03
ϵ	$=\rho$	$\frac{1}{2} = 0.5$	0.536 ± 0.007	$\frac{2}{3} \approx 0.667$	0.63 ± 0.01	$\frac{5}{9} \approx 0.556$	0.57 ± 0.02	0.554 ± 0.006
ν_{path}	…	$\frac{1}{2} = 0.5$	0.509 ± 0.009	$\frac{3}{4} = 0.75$	0.780 ± 0.005	$\frac{3}{5} = 0.6$	0.593 ± 0.007	0.565 ± 0.007
ν	$=\rho\,\nu_{\text{path}}$	$\frac{1}{4} = 0.25$	0.25 ± 0.02	$\frac{1}{2} = 0.5$	0.48 ± 0.02	$\frac{1}{3} \approx 0.333$	0.32 ± 0.02	0.29 ± 0.01
θ_{path}	…	…	−0.04 ± 0.04	…	0.65 ± 0.06	…	0.12 ± 0.05	0.14 ± 0.02

averages of all independent measurements. Corresponding uncertainties are given in the form ±(statistical error) ±(systematic error), where the "statistical error" is the largest value obtained from the different fits[36] while the "systematic error" is the spread between the single estimates, respectively. In those cases where Eq. (24) fails producing trustable results we have retained only the 2-parameter fit, Eq. (23), and a separate analysis of uncertainties was required, see the caption of Table SVII for details. Error bars reported in Table I are given by $\sqrt{(\text{statistical error})^2 + (\text{systematic error})^2}$.

IV. RESULTS

In Secs. IV A–IV F, we discuss the structure of trees in $2d$ and $3d$ melts by considering the scaling behaviors of the observables defined in Sec. II B and their corresponding critical exponents. Following the general outline and using results from our previous work,[17] we compare the properties of interacting trees to those of corresponding ideal trees.

A. Branching statistics for trees with annealed connectivity

Our results for the average number of branch points, $\langle n_3(N)\rangle$, as a function of N are listed in Tables SII and SIII. Figure 3 shows that the ratios of 3-functional nodes, $\langle n_3(N)\rangle/N$, reach their asymptotic value already for moderate tree weights. Interestingly, our results for ideal trees as well as interacting trees perfectly agree to each other with asymptotic branching probability[17] $\lambda = \lim_{N\to\infty}\langle n_3(N)\rangle/N = 0.4$. In fact, due to the multiple occupation of lattice sites in the melt, the branching probabilities remain virtually unchanged in spite of the interactions. Corresponding distributions $p(n_3)$ are well described by Gaussian statistics with corresponding variances increasing linearly with N, see Fig. S2.

B. Path length statistics for trees

Our results for (A) the mean contour distance between pairs of nodes, $\langle L(N)\rangle$, (B) the mean contour distance of nodes from the central node, $\langle \delta L_{\text{center}}(N)\rangle$, and (C) the mean *longest* contour distance of nodes from the central node, $\langle \delta L^{\max}_{\text{center}}(N)\rangle$ are summarized in Tables SII-III and plotted in Figs. 4 and S3. As discussed in Sec. II B, the three quantities are expected to scale with the total tree weight N as $\langle \delta L_{\text{center}}(N)\rangle \sim \langle \delta L^{\max}_{\text{center}}(N)\rangle \sim \langle L(N)\rangle \sim N^{\rho}$. Extracted single values for ρ's including more details on their statistical significance (χ^2 and Q-values) are summarized in Table SIV. Our final best estimates for ρ's (straight lines in Fig. 4 and Fig. S3, and Tables I and SIV) are obtained by combining the corresponding results for $\langle \delta L_{\text{center}}(N)\rangle$, $\langle \delta L^{\max}_{\text{center}}(N)\rangle$, and $\langle L(N)\rangle$.

C. Path lengths vs. weights for branches

The relation between branch weight and path length can also be explored on the level of branches. We have analyzed the scaling behavior of (1) the average branch weight, $\langle N_{br}(\delta l^{\max}_{\text{root}})\rangle$, as a function of the longest contour distance to the branch root, $\delta l^{\max}_{\text{root}}$, and (2) the average branch (or tree core) weight, $\langle N_{\text{center}}(\delta l_{\text{center}})\rangle$, inside a contour distance δl_{center} from the central node of the tree. Corresponding results are shown in Fig. 5. Both data sets show universal behavior at intermediate $\delta l^{\max}_{\text{root}}$ and δl_{center}, and saturate to the corresponding expected limiting values $=\frac{N-1}{2}$ and $=N$. For large $\delta l^{\max}_{\text{root}}$ (respectively, δl_{center}) the relation $\langle N_{br}(\delta l^{\max}_{\text{root}})\rangle \sim \delta l^{\max 1/\rho}_{\text{root}}$ (respectively, $\langle N_{\text{center}}(\delta l_{\text{center}})\rangle \sim \delta {l_{\text{center}}}^{1/\rho}$) is expected to hold. For N_{br} (and with an analogous expression for N_{center}), we have estimated ρ as $\rho(\delta l^{\max}_{\text{root}}) = \left(\frac{\log\langle N_{br}(\delta l^{\max}_{\text{root}}+1)\rangle/\langle N_{br}(\delta l^{\max}_{\text{root}})\rangle}{\log(\delta l^{\max}_{\text{root}}+1)/\delta l^{\max}_{\text{root}}}\right)^{-1}$. Numerical results are reported in the corresponding insets of Fig. 5, the large-scale behaviour agreeing well with the best estimates for ρ's (horizontal lines) summarized in Table I.

D. Branch weight statistics

The scaling behavior of the average branch weight, $\langle N_{br}(N)\rangle \sim N^{\epsilon}$, defines the critical exponent ϵ. Single values of $\langle N_{br}(N)\rangle$ for each N (see Tables SII and SIII) are plotted in Fig. 6, where the straight lines have slopes corresponding

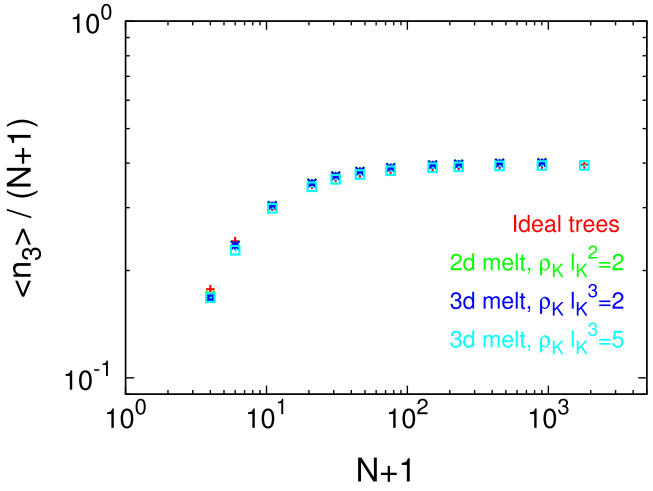

FIG. 3. Branching statistics. Average fraction of 3-functional nodes, $\frac{\langle n_3\rangle}{N+1}$, as a function of the total number of tree nodes, $N+1$. The asymptotic branching probability[17] λ is =0.4.

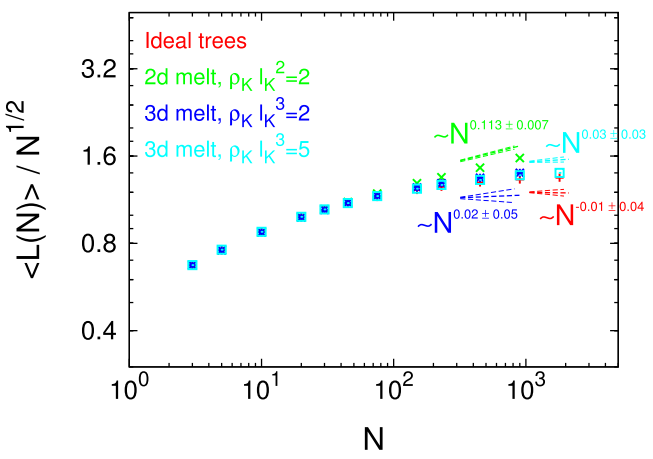

FIG. 4. Path length statistics. Mean contour distance between pairs of nodes, $\langle L(N)\rangle$. Straight lines correspond to the large-N behaviour $\langle L(N)\rangle \sim N^{\rho}$ with critical exponents ρ given by the best estimates summarised in Table I.

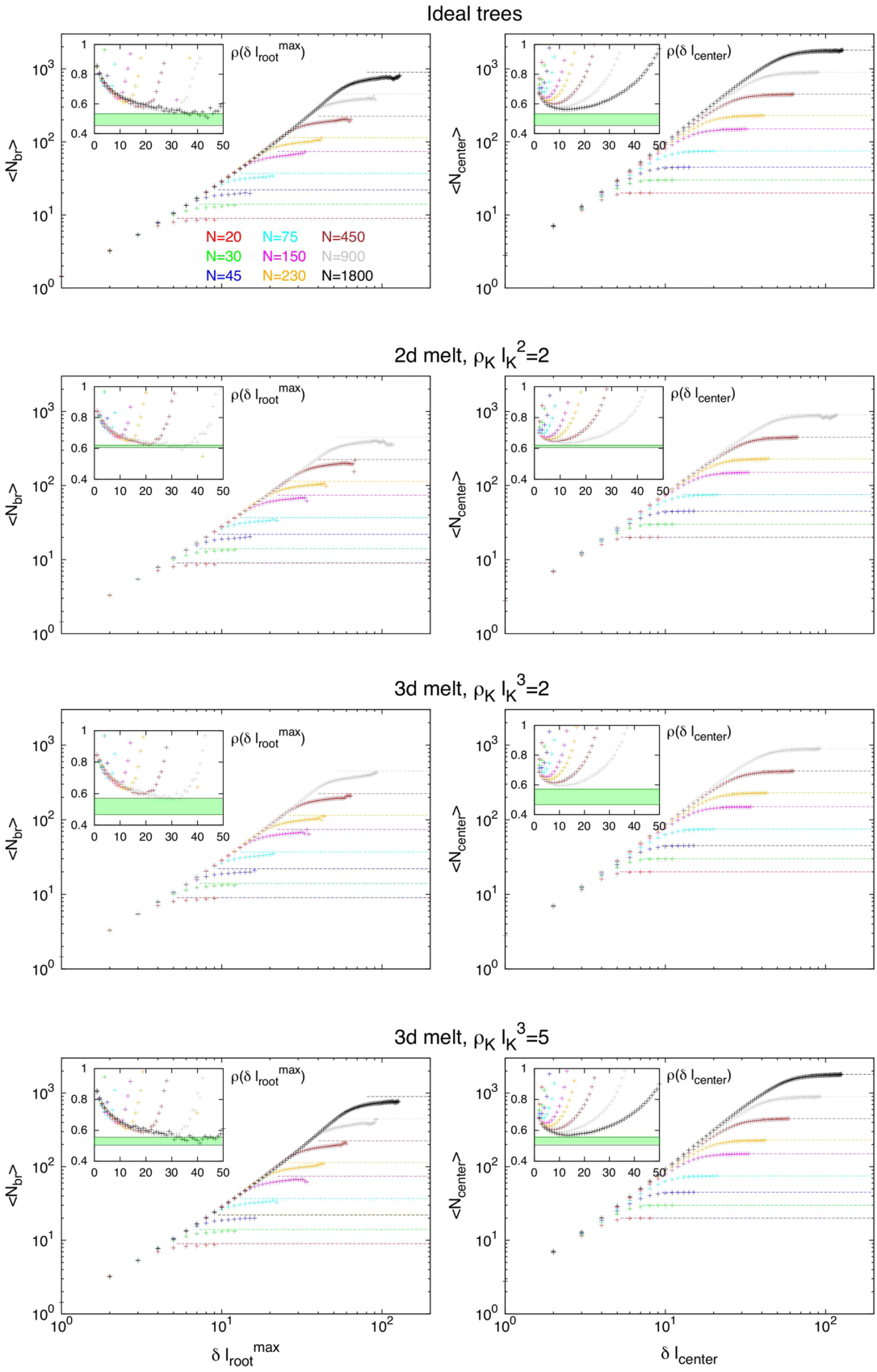

FIG. 5. Path lengths vs. weights of branches. Data for trees of weight from $N = 20$ to $N = 1800$. (Left) Average branch weight, $\langle N_{br}(\delta l_{\rm root}^{\rm max})\rangle$, as a function of the longest contour distance to the branch root, $\delta l_{\rm root}^{\rm max}$. For large $\delta l_{\rm root}^{\rm max}$, curves saturate to the corresponding maximal branch weight $(N-1)/2$ (dashed horizontal lines). (Right) Average branch weight, $\langle N_{\rm center}(\delta l_{\rm center})\rangle$, composed of segments whose distance from the central node does not exceed $\delta L_{\rm center}$. For large $\delta l_{\rm center}$, curves saturate to the corresponding total tree weight, N (dashed horizontal lines). Insets: Corresponding differential fractal exponent $\rho(\delta l_{\rm root}^{\rm max})$ and $\rho(\delta l_{\rm center})$. Shaded regions show the range of ρ values summarized in Table I. First row panels are as in Ref. 17, and reproduced with permission from A. Rosa and R. Everaers, J. Phys. A: Math. Theor. **49**, 345001 (2016). Copyright 2016 IOP Publishing Ltd.

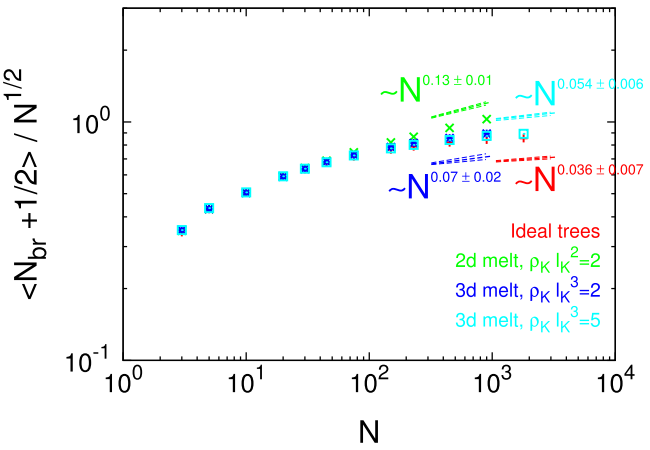

FIG. 6. Branch weight statistics. Average branch weight, $\langle N_{br}(N)\rangle$ as a function of the total tree mass, N. Straight lines correspond to the large-N behaviour $\langle N_{br}(N)\rangle \sim N^{\epsilon}$ with critical exponents ϵ given by the best estimates summarised in Table I.

to our best estimates for ϵ's (Table I), see also Table SIV for details. We notice, in particular, that the scaling relation $\rho = \epsilon$ holds within error bars.

E. Conformational statistics of linear paths

In order to extract the critical exponent ν_{path} which defines the scaling behavior $\langle R^2(l,N)\rangle \sim l^{2\nu_{\text{path}}}$, we have selected paths of length close to the average length ($l = \langle L(N)\rangle$) and to the trees maximal length ($l = L_{\max}(N)$) and calculated corresponding mean-square end-to-end distances $\langle R^2(\langle L\rangle)\rangle \sim \langle L(N)\rangle^{2\nu_{\text{path}}}$ and $\langle R^2(L_{\max})\rangle \sim \langle L_{\max}(N)\rangle^{2\nu_{\text{path}}}$ (see Fig. 7 and corresponding tabulated values in Tables SV and SVI). Combination of the two (Table SVII) led to our best estimates for ν_{path} in the different ensembles summarized in Table I. Not surprisingly, these values agree well with the differential exponents $\nu_{\text{path}}(l) = \frac{1}{2}\frac{\log\langle R^2(l+1,N)\rangle/\langle R^2(l,N)\rangle}{\log(l+1)/l}$ reported in the l.h.s insets of Fig. 8.

Then, we have calculated the mean closure probabilities, $\langle p_c(l,N)\rangle$ (Fig. 8, right-hand panels), normalised to the corresponding "mean-field" expectation values $\langle R^2(l,N)\rangle^{-3/2} \sim l^{-3\nu_{\text{path}}}$. As in the case of single self-avoiding trees in good solvent,[17] $\langle p_c(l,N)\rangle$ for interacting trees markedly deviate from the mean-field prediction, which defines a *novel* critical exponent θ_{path}, $\langle p_c(l,N)\rangle\langle R^2(l,N)\rangle^{3/2} \sim l^{-\nu_{\text{path}}\theta_{\text{path}}}$. Estimated values for θ_{path}'s are reported in Table I.

F. Conformational statistics of trees

Finally, we have measured the mean-square gyration radius, $\langle R_g^2(N)\rangle$ (tabulated values in Tables SV and SVI), and the average shape of trees as a function of tree weight, N (Fig. 9, panels (a) and (b) respectively). Estimated values of critical exponents ν (straight lines in Fig. 9(a)) are summarized in Table I, while details about their derivation are given in Table SVII.

V. DISCUSSION

We have analyzed the behavior of interacting trees with annealed connectivity in $2d$ and $3d$ melts in terms of a small set of exponents defined in the Introduction and in Sec. II B. With weights of up to $N = 1800$ segments, our tree sizes are comparable to those of linear chains in similar studies.[43–45] However, for many purposes the average contour distance, $\langle L\rangle \le O(100) \ll N$, between monomers provides a more suitable comparison. The reader should thus bear in mind, that extracted exponents are either (i) effective (crossover) exponents valid for the particular systems and system sizes we have studied or (ii) *estimates* of true, asymptotic exponents, which suffer from uncertainties related to the extrapolation to the asymptotic limit. These effects are particularly pronounced for the high density $3d$ melts we studied in Ref. 16. For example, we initially reported[16] the results of a simple power law fit including all data for tree sizes $N \ge 75$ suggesting $\nu = 0.32 \pm 0.01$. In contrast, the present more refined analysis yields $\nu = 0.29 \pm 0.01$. If this result is acceptable as an effective exponent for tree sizes $N = O(1000)$, it mostly illustrates that one cannot extract the asymptotic behaviour assuming a *single*, small correction to scaling, if the available tree sizes barely reach the crossover (Sec. II E). The discussion below focuses on results for lower density $2d$ and $3d$ melts, where the studied tree sizes are significantly larger than the estimated blob size.

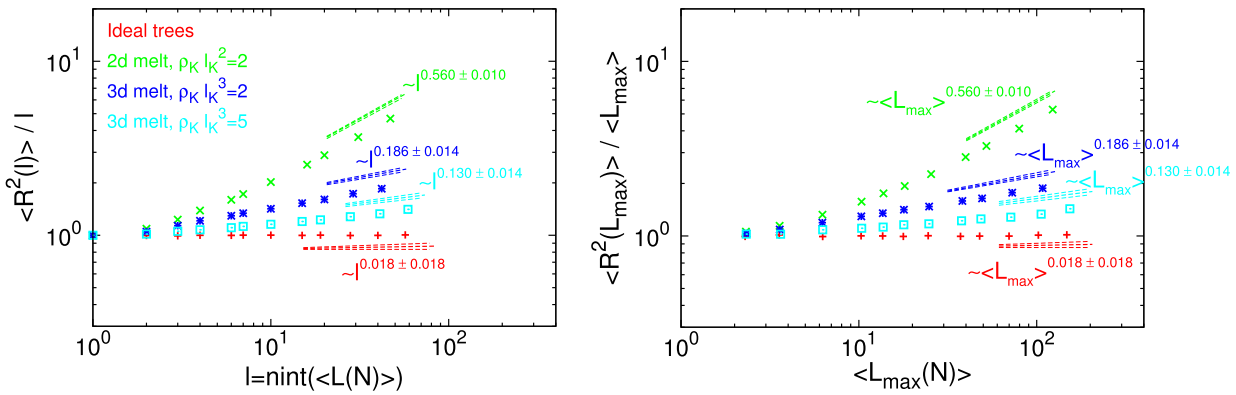

FIG. 7. Conformational statistics of linear paths. (Left) Mean-square end-to-end distance, $\langle R^2(\ell = \texttt{nint}(\langle L\rangle))\rangle$, of paths of length $\ell = \texttt{nint}(\langle L(N)\rangle)$ ≡ closest-integer-to $\langle L(N)\rangle$. (Right) Mean-square end-to-end distance, $\langle R^2(L_{\max})\rangle$, of the longest paths. Straight lines correspond to the large-ℓ or large-$\langle L_{\max}(N)\rangle$ behaviours: $\langle R^2(\ell)\rangle \sim \ell^{2\nu_{\text{path}}}$ or $\langle R^2(L_{\max})\rangle \sim \langle L_{\max}(N)\rangle^{2\nu_{\text{path}}}$. Critical exponents ν_{path} are given by the best estimates reported in Table I.

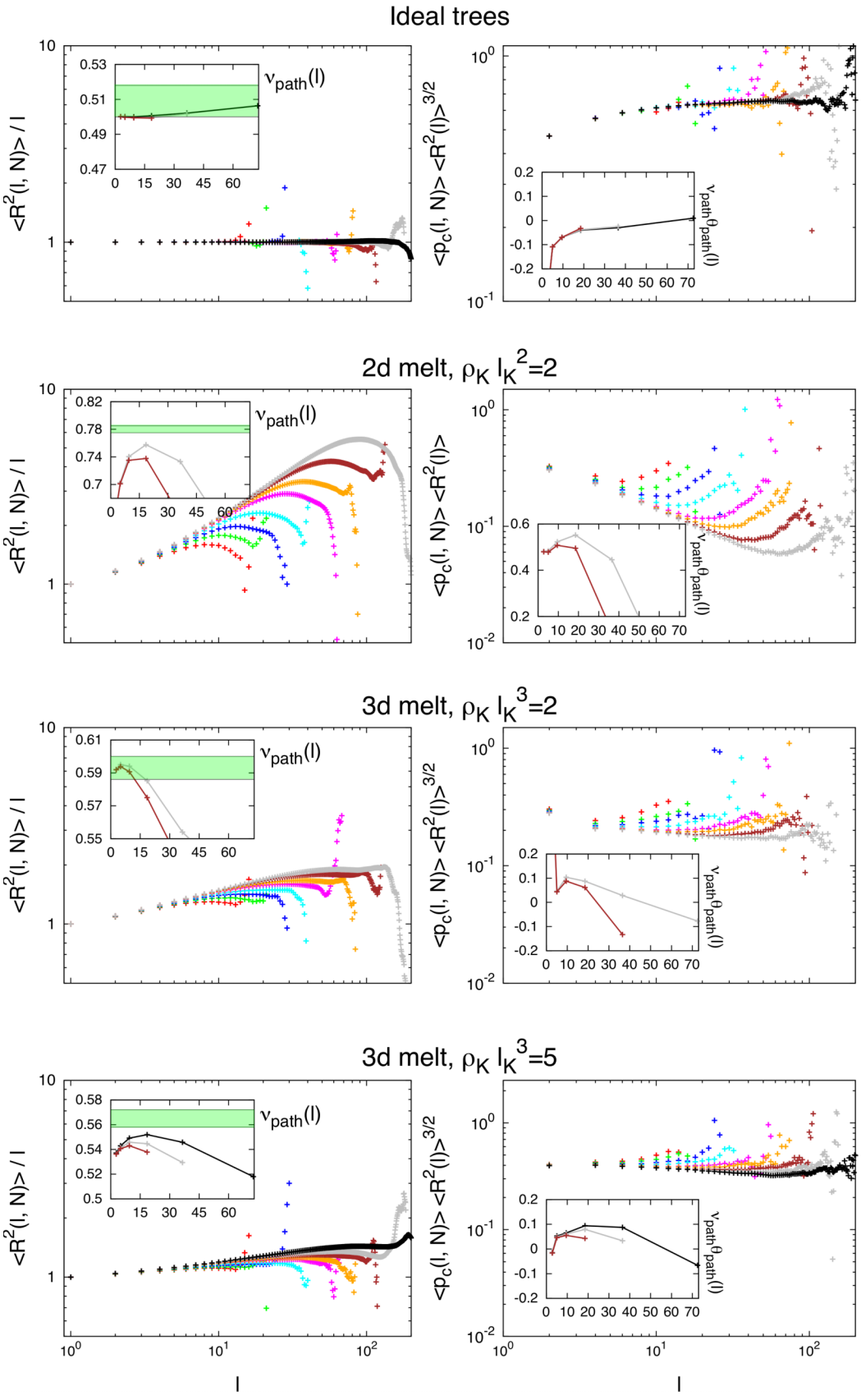

FIG. 8. Conformational statistics of linear paths. (Left column) Mean-square end-to-end distance, $\langle R^2(l,N)\rangle$, of linear paths of length l. Insets: Differential fractal exponent, $\nu_{\text{path}}(l) = \frac{1}{2}\frac{\log\langle R^2(l+1,N)\rangle/\langle R^2(l,N)\rangle}{\log(l+1)/l}$ for chain lengths $N \geq 450$. Shaded regions show the range of ν_{path} values summarized in Table I. (Right column) Mean closure probabilities, $\langle p_c(l,N)\rangle$, between ends of linear paths of length l normalised to the mean-field expectation value $\langle R^2(l,N)\rangle^{-3/2}$. Insets: Differential fractal exponent $\nu_{\text{path}}\theta_{\text{path}}(l)$, see Eq. (5), defined analogously to $\nu_{\text{path}}(l)$ for chain lengths $N \geq 450$. Plots in the insets have been obtained by averaging corresponding quantities over log-spaced intervals. Color code is as in Fig. 5. First row panels are as in Ref. 17, and reproduced with permission from A. Rosa and R. Everaers, J. Phys. A: Math. Theor. **49**, 345001 (2016). Copyright 2016 IOP Publishing Ltd.

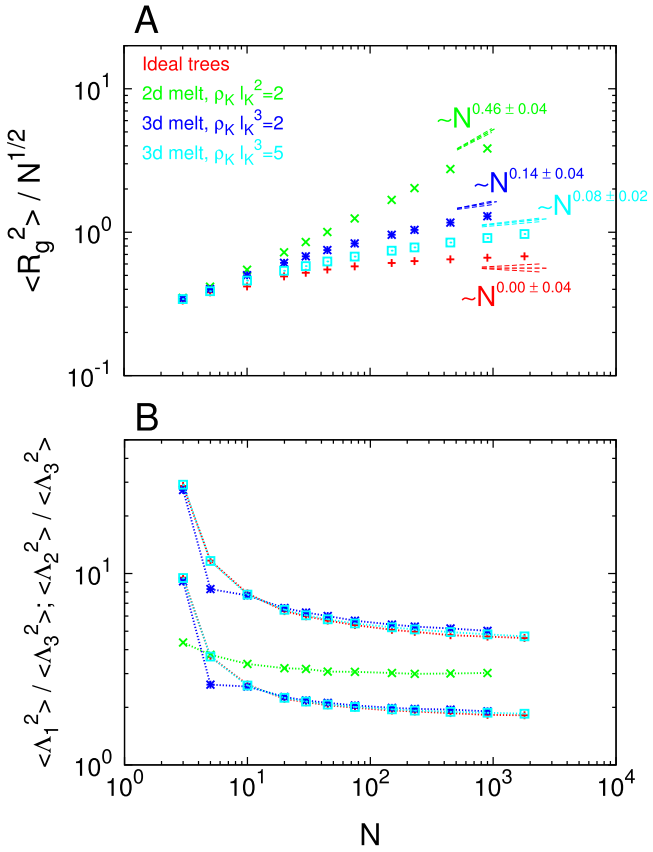

FIG. 9. Conformational statistics of trees. (a) Mean square gyration radius, $\langle R_g^2(N)\rangle$. Straight lines correspond to the large-N behaviour $\langle R_g^2(N)\rangle \sim N^{2\nu}$ with critical exponents ν given by the best estimates summarised in Table I. (b) Tree average aspect ratios, $\langle\Lambda_1^2\rangle/\langle\Lambda_3^2\rangle$ and $\langle\Lambda_2^2\rangle/\langle\Lambda_3^2\rangle$.

Our results are summarised in Table I. Most of them are in quantitative or at least good qualitative agreement with the predictions from the Flory theory.[1,15,30,31] First, this implies that the reported exponents ν_{path} for melts of trees fit to the predicted[15] value $\frac{3}{d+2}$ which, intriguingly, corresponds to the Flory[46] exponent ν for self-avoiding *linear* chains in good solvent conditions. Second, the results for the exponent ν are in agreement with the prediction $\nu = 1/d$ and confirm that trees in melts behave as "territorial" polymers. This result is relatively simple to understand as $\nu = 1/d$ represents the minimal amount of swelling compatible with steric packing requirements. Thus not too much stock should be put in the fact that the Flory value for ν turns out to be exact in the present case. More interestingly, the theory makes two testable, non-trivial predictions for the contributions of connectivity changes and path stretching to the overall swelling[31] (Eqs. (13) and (14)): first, both effects should only depend on the magnitude of the overall swelling, but not its physical origin, and second path stretching is expected to be dominant as[47] $\nu_{\text{path}} - \nu_{\text{path}}^{\text{ideal}} \approx 2(\rho - \rho^{\text{ideal}}) = 4(\nu - \nu^{\text{ideal}})/3$ for weakly swollen trees. The first prediction is well borne out by the comparison of $3d$ self-avoiding trees and $2d$ melt trees. In both cases, the trees are expected to swell to $\nu = 1/2$. Interestingly, the observed values for ρ and ν_{path} turn out to be almost identical and close to the predicted values. The second prediction is confirmed by noticing that trees in $2d$ and $3d$ melts swell almost exclusively at the path level (Fig. 7), while the observed modifications of the connectivities (Figs. 4 and 6) are very weak. In absolute terms for our largest trees with $N = 900$ (see Tables SII, SIII, SV, and SVI) $\langle R_g^2\rangle_{2d\ \text{melt}}/\langle R_g^2\rangle_{\text{ideal}} = 5.78 \pm 0.03$, $\langle R^2(L_{\max})\rangle_{2d\ \text{melt}}/\langle R^2(L_{\max})\rangle_{\text{ideal}} = 6.32 \pm 0.10$, and $\langle L\rangle_{2d\ \text{melt}}/\langle L\rangle_{\text{ideal}} = 1.188 \pm 0.002$ while $\langle R_g^2\rangle_{3d\ \text{melt}}/\langle R_g^2\rangle_{\text{ideal}} = 1.95 \pm 0.02$, $\langle R^2(L_{\max})\rangle_{3d\ \text{melt}}/\langle R^2(L_{\max})\rangle_{\text{ideal}} = 1.96 \pm 0.03$, and $\langle L\rangle_{3d\ \text{melt}}/\langle L\rangle_{\text{ideal}} = 1.054 \pm 0.003$.

For other quantities, Flory theory is even qualitatively wrong. A particularly interesting case are the average contact probability $\langle p_c(l)\rangle$ between nodes at path distance l. As shown in Fig. 8 and Table I, $\langle p_c(l)\rangle$'s for interacting trees deviate consistently from the naïve mean-field estimate of $l^{-3\nu_{\text{path}}}$. This is yet another illustration of the subtle cancellation of errors in Flory arguments, which are built on the mean-field estimates of contact probabilities.[26]

VI. SUMMARY AND CONCLUSION

Motivated by the close analogy between non-concatenated ring polymers and annealed lattice trees,[11–13,15,16] we have studied the statistical properties of tree melts in $d = 2$ and $d = 3$ dimensions. We have used the same methodology as in our recent work on self-avoiding trees,[17] i.e., variants of the amoeba[2] and burning[40,41] algorithms for the Monte Carlo simulation and the connectivity analysis (Sec. III). Table I summarises our estimates of the asymptotic values of the exponents describing the scaling behavior of the average branch weight, $\langle N_{br}(N)\rangle \sim N^{\epsilon}$, the average path length, $\langle L(N)\rangle \sim N^{\rho}$, the mean-square path extension, $\langle R^2(l)\rangle \sim l^{2\nu_{\text{path}}}$, and the tree and branch gyration radii, $\langle R_g^2(N)\rangle \sim N^{2\nu}$ (Sec. IV). Our results are in excellent agreement with an asymptotic scaling of the average tree size of $R \sim N^{1/d}$, suggesting that the trees behave as compact, *territorial*[48] fractals (Fig. 9). Moreover, we find that the trees swell by the combination of modified branching and path stretching. However, the former effect is subdominant and difficult to detect in $d = 3$ dimensions.

Our results for dense systems contribute to the evidence suggesting that Flory theory[1,15,30,31] provides a useful framework for discussing the behavior of interacting trees. That Flory theory should work for trees is not a foregone conclusion. In the case of linear chains, the approach is notorious (and appreciated) for the nearly perfect cancellation of large errors in the estimation of *both* terms in Eq. (11).[26,32] This delicate balance might well have been destroyed for trees, where the Flory energy needs to be simultaneously minimized with respect to L and R. In two forthcoming publications, we will generalise Flory theory to trees of finite size and extensibility,[34] and we will analyse the distribution functions for the quantities whose *mean* behaviour we have explored in this work and in Ref. 17, in an attempt to go beyond the Flory theory.[35]

SUPPLEMENTARY MATERIAL

See supplementary material for complementary figures and tables cited in the article.

ACKNOWLEDGMENTS

AR acknowledges Grant No. PRIN 2010HXAW77 (Ministry of Education, Italy). RE is grateful for the hospitality of the Kavli Institute for Theoretical Physics (Santa Barbara, USA) and support through the National Science Foundation under Grant No. NSF PHY11-25915 during his visit in 2011, which motivated the present work. In particular, we have benefited from long and stimulating exchanges with M. Rubinstein and A. Yu. Grosberg on the theoretical background. This work was only possible by generous grants of computer time by PSMN (ENS-Lyon), in part through the equip@meso facilities of the FLMSN.

[1]J. Isaacson and T. C. Lubensky, "Flory exponents for generalized polymer problems," J. Phys., Lett. **41**, L469–L471 (1980).
[2]W. A. Seitz and D. J. Klein, "Excluded volume effects for branched polymers," J. Chem. Phys. **75**, 5190–5193 (1981).
[3]J. A. M. S. Duarte and H. J. Ruskin, "The branching of real lattice trees as dilute polymers," J. Phys. **42**, 1585–1590 (1981).
[4]G. Parisi and N. Sourlas, "Critical behavior of branched polymers and the Lee-Yang edge singularity," Phys. Rev. Lett. **46**, 871–874 (1981).
[5]M. E. Fisher, "Yang-Lee edge singularity and ϕ^3 field-theory," Phys. Rev. Lett. **40**, 1610–1613 (1978).
[6]D. A. Kurtze and M. E. Fisher, "Yang-Lee edge singularities at high-temperatures," Phys. Rev. B **20**, 2785–2796 (1979).
[7]A. Bovier, J. Fröhlich, and U. Glaus, "Branched polymers and dimensional reduction," in *Critical Phenomena, Random Systems, Gauge Theories*, edited by K. Osterwalder and R. Stora (North-Holland, Amsterdam, 1984).
[8]P. Bacova, L. G. D. Hawke, D. J. Read, and A. J. Moreno, "Dynamics of branched polymers: A combined study by molecular dynamics simulations and tube theory," Macromolecules **46**, 4633–4650 (2013).
[9]M. Rubinstein and R. H. Colby, *Polymer Physics* (Oxford University Press, New York, 2003).
[10]W. Burchard, "Solution properties of branched macromolecules," Adv. Polym. Sci. **143**, 113 (1999).
[11]A. R. Khokhlov and S. K. Nechaev, "Polymer chain in an array of obstacles," Phys. Lett. **112A**, 156–160 (1985).
[12]M. Rubinstein, "Dynamics of ring polymers in the presence of fixed obstacles," Phys. Rev. Lett. **57**, 3023–3026 (1986).
[13]S. P. Obukhov, M. Rubinstein, and T. Duke, "Dynamics of a ring polymer in a gel," Phys. Rev. Lett. **73**, 1263–1266 (1994).
[14]M. Kapnistos *et al.*, "Unexpected power-law stress relaxation of entangled ring polymers," Nat. Mater. **7**, 997 (2008).
[15]A. Yu. Grosberg, "Annealed lattice animal model and flory theory for the melt of non-concatenated rings: Towards the physics of crumpling," Soft Matter **10**, 560–565 (2014).
[16]A. Rosa and R. Everaers, "Ring polymers in the melt state: The physics of crumpling," Phys. Rev. Lett. **112**, 118302 (2014).
[17]A. Rosa and R. Everaers, "Computer simulations of randomly branching polymers: Annealed vs. quenched branching structures," J. Phys. A: Math. Theor. **49**, 345001 (2016).
[18]A. Grosberg, Y. Rabin, S. Havlin, and A. Neer, "Crumpled globule model of the three-dimensional structure of DNA," Europhys. Lett. **23**, 373–378 (1993).
[19]A. Rosa and R. Everaers, "Structure and dynamics of interphase chromosomes," PLoS Comput. Biol. **4**, e1000153 (2008).
[20]T. Vettorel, A. Y. Grosberg, and K. Kremer, "Statistics of polymer rings in the melt: A numerical simulation study," Phys. Biol. **6**, 025013 (2009).
[21]L. A. Mirny, "The fractal globule as a model of chromatin architecture in the cell," Chromosome Res. **19**, 37–51 (2011).
[22]M. Lang, "Ring conformations in bidisperse blends of ring polymers," Macromolecules **46**, 1158–1166 (2013).
[23]J. Smrek and A. Yu. Grosberg, "Minimal surfaces on unconcatenated polymer rings in melt," ACS Macro Lett. **5**, 750–754 (2016).
[24]M. E. Cates and J. M. Deutsch, "Conjectures on the statistics of ring polymers," J. Phys. (Paris) **47**, 2121–2128 (1986).
[25]T. Ge, S. Panyukov, and M. Rubinstein, "Self-similar conformations and dynamics in entangled melts and solutions of nonconcatenated ring polymers," Macromolecules **49**, 708–722 (2016).
[26]P.-G. De Gennes, *Scaling Concepts in Polymer Physics* (Cornell University Press, Ithaca, 1979).
[27]M. Doi and S. F. Edwards, *The Theory of Polymer Dynamics* (Oxford University Press, New York, 1986).
[28]A. Yu. Grosberg and A. R. Khokhlov, *Statistical Physics of Macromolecules* (AIP Press, New York, 1994).
[29]B. H. Zimm and W. H. Stockmayer, "The dimensions of chain molecules containing branches and rings," J. Chem. Phys. **17**, 1301–1314 (1949).
[30]M. Daoud and J. F. Joanny, "Conformation of branched polymers," J. Phys. **42**, 1359–1371 (1981).
[31]A. M. Gutin, A. Yu. Grosberg, and E. I. Shakhnovich, "Polymers with annealed and quenched branchings belong to different universality classes," Macromolecules **26**, 1293–1295 (1993).
[32]J. des Cloizeaux and G. Jannink, *Polymers in Solution* (Oxford University Press, Oxford, 1989).
[33]R. Everaers, A. Yu. Grosberg, M. Rubinstein, and A. Rosa, "Flory theory of randomly branching polymers I: Asymptotic behaviour" (unpublished).
[34]R. Everaers, "Flory theory of randomly branching polymers II: Interacting trees of finite size and finite extensibility" (unpublished).
[35]A. Rosa and R. Everaers, "Beyond Flory theory: Distribution functions for interacting lattice trees" (unpublished), e-print arXiv.org/abs/1610.05230.
[36]E. J. Janse van Rensburg and N. Madras, "A nonlocal Monte Carlo algorithm for lattice trees," J. Phys. A: Math. Gen. **25**, 303–333 (1992).
[37]P. J. Flory, *Principles of Polymer Chemistry* (Cornell University Press, Ithaca, NY, 1953).
[38]A. Yu. Grosberg and S. K. Nechaev, "From statistics of regular tree-like graphs to distribution function and gyration radius of branched polymers," J. Phys. A: Math. Theor. **48**, 345003 (2015).
[39]The result is consistent with the "traditional" picture[9] that polymers in semi-dilute solutions can be represented as chains of blobs, where each blob contains g monomers and has a linear size $R(g) \sim l_K g^{\nu}$. Since blobs are densily packed,[9] the monomer density inside each blob equals the overall density or, neglecting prefactors, $\rho_K \sim g/R(g)^3 \to g \sim (\rho_K l_K^3)^{1/(1-3\nu)}$. For standard semi-dilute solutions of linear chains, $\nu \approx 0.6$ and $g \sim (\rho_K l_K^3)^{-1.25}$ decreases with density.[9] For our melts of trees, $\nu = 1/4$ (see Fig. 9(a)) and $g \sim (\rho_K l_K^3)^4$ (equivalent within numerical prefactors to Eq. (20)) which increases with density. This picture ought to break when density fluctuations (see discussion at the end of Sec. II A) become comparable to ρ_K, or $\rho_K l_K^3 \approx \sqrt{0.13} \approx 0.4$.
[40]H. J. Heermann, D. C. Hong, and H. E. Stanley, "Backbone and elastic backbone of percolation clusters obtained by the new method of 'burning,'" J. Phys. A: Math. Gen. **17**, L261–L266 (1984).
[41]D. Stauffer and A. Aharony, *Introduction to Percolation Theory* (Taylor & Francis Inc., 1994).
[42]W. H. Press, S. A. Teukolsky, W. T. Vetterling, and B. F. Flannery, *Numerical Recipes in Fortran*, 2nd ed. (Cambridge University Press, Cambridge, 1992).
[43]H. Meyer, J. P. Wittmer, T. Kreer, A. Johner, and J. Baschnagel, "Static properties of polymer melts in two dimensions," J. Chem. Phys. **132**, 184904 (2010).
[44]J. P. Wittmer *et al.*, "Scale-free static and dynamical correlations in melts of monodisperse and flory-distributed homopolymers," J. Stat. Phys. **145**, 1017–1126 (2011).
[45]N. Schulmann, H. Meyer, J. P. Wittmer, A. Johner, and J. Baschnagel, "Inter-chain monomer contact probability in two-dimensional polymer solutions," Macromolecules **45**, 1646–1651 (2012).
[46]P. J. Flory, *Statistical Mechanics of Chain Molecules* (Interscience, New York, 1969).
[47]The result is trivially obtained by expanding Eqs. (13) and (14) around the ideal values $\nu_{\text{path}}^{\text{ideal}} = \rho_{\text{path}}^{\text{ideal}} = 1/2$ and $\nu^{\text{ideal}} = 1/4$.
[48]T. Vettorel, A. Y. Grosberg, and K. Kremer, "Territorial polymers," Phys. Today **62**, 72 (2009).